P. Panicucci, B. Bercovici, E. Zenou, J. Mcmahon, M. Delpech, J. Lebreton, K. Kanani
Uncertainties in the Gravity Spherical Harmonics Coefficients Arising from a Stochastic Polyhedral Shape
Celestial Mechanics and Dynamical Astronomy, Vol. 132, N. 4, 2020, 23 (27 pages)
doi:10.1007/s10569-020-09962-8

Noname manuscript No.
(will be inserted by the editor)

Uncertainties in the gravity spherical harmonics coefficients arising from a stochastic polyhedral shape

Paolo Panicucci [1,2,3], Benjamin Bercovici [4], Emmanuel Zenou [1], Jay McMahon [4], Michel Delpech [2], Jérémy Lebreton [3], and Keyvan Kanani [3]

[1]ISAE-SUPAERO, Toulouse, France
[2]Centre National d'Études Spatiales, France
[3]Airbus Defence & Space, France
[4]University of Colorado, Boulder, USA

the date of receipt and acceptance should be inserted later

Abstract The increasing interest towards exploring small bodies in the Solar System has paved the way for the investigation of different gravity field models allowing robust orbit design and dynamical environment characterization. Among these, the spherical harmonics representation and the polyhedral gravity model are the most employed and studied - the former for historical reasons and the latter due to the fact that it is an exact and closed-form representation of the gravity field arising from a constant-density polyhedron. The exact algorithm computing the spherical harmonics coefficients from a given polyhedron is available in the literature. Unfortunately, little to no insight into the uncertainty in the spherical harmonics coefficients is provided alongside their computed value, as the polyhedron is customarily considered as a deterministically known solid. During orbit design, spacecraft operations and small body characterization, it is crucial to account for the uncertainty in the spherical harmonics coefficients and whether it influences the overall mission architecture. This paper provides the analytical derivation of the partial derivatives of the transformation between the constant density polyhedron and the spherical harmonics coefficients with respect to the vertices of the polyhedron. This derivation allows for the quantification of the spherical harmonics coefficients uncertainties when a stochastic polyhedral shape is considered, i.e. a shape whose vertices do not have a deterministic position. As a result, the analytical expressions of the uncertainty in the gravity potential and acceleration are assembled to rigorously quantify the influence of a stochastic polyhedron on the surrounding dynamical environment. A brief explanation of the implementation procedure and the polyhedron vertices covariance matrix definition is provided to the reader. The final result of the paper is a set of numerical simulations validating the proposed model and demonstrating its capability to provide the uncertainties in the spherical harmonics coefficients, the gravity potential and acceleration arising from a stochastic polyhedral shape.

Keywords Spherical Harmonics · Uncertainty Quantification · Small Body Gravity · Stochastic Shape

paolo.panicucci@isae-supaero.fr

bebe0705@colorado.edu

emmanuel.zenou@isae-supaero.fr

jay.mcmahon@colorado.edu

Michel.Delpech@cnes.fr

jeremy.lebreton@airbus.com

keyvan.kanani@airbus.com

Address(es) of author(s) should be given

1 Introduction and motivations

Exterior spherical harmonics, from now on simply called spherical harmonics, are a classical representation of the gravity field around planets and small bodies. Their mathematical foundation relies on the possibility to project, in the L_2-sense, a function defined on the sphere Ω on an orthogonal functional basis of $L_2(\Omega)$, such as the associated Legendre polynomials [1, 2]. The strength of this approach relies on the limited number of constant coefficients that are needed to represent the gravity field of a body with a tunable precision. This is mainly due to the global spatial localization of the spherical harmonics expansion kernel and its punctual localization in the frequency domain [3]. Its main limitation is the non-convergence to the right series inside the Brillouin sphere, defined as the body-circumscribing sphere centered at its center of mass. This is due to the mathematical definition of the region of convergence of Legendre polynomials expansions [4, 5]. For Earth or almost-spherical planetary applications, this issue is of minor importance as the Brillouin sphere is almost coincident with the planet surface or, otherwise, the possible existence of an atmosphere makes such low altitudes uninteresting from an astrodynamics perspective. However, this divergence issue does manifest itself about small bodies of the Solar System and, as a consequence, other gravity field representations have been proposed to overcome this limitation [6–8]. Werner and Scheeres's polyhedral gravity model is the state-of-the-art approach to represent the gravity field of non-spherical bodies as it is a closed and analytical form of the gravity field that verifies the Laplace equation everywhere outside the body and it is well-defined everywhere but on the polyhedral edges. Unfortunately, the number of parameter to represent the gravity field is very high as it is the vertices and the associated connectivity matrix, i.e. a matrix associating each facet to the correct vertices. Moreover, the evaluation of the gravity field in a point around the body is computationally costly as it implies the iteration over each vertex and each facet. Furthermore, it does not provide a straightforward and "visual" insight about density and the body mass distribution. For these reasons, the spherical harmonics representation is still a compelling and employed gravity field modeling for deep-space navigators, mission designers and scientists [9–13].

It must be noted that a satellite must orbit around the small body under the influence of its gravity by knowing accurately the satellite position to estimate the spherical harmonics coefficients without considering the contribution of the small body shape. When this is not possible, the spherical harmonics coefficients can be estimated from the shape by knowing the small body density. If the coefficients are estimated from the orbit determination solution, the coupling with the shape provides a fruitful insight on the mass distribution of the body with respect to a uniform density [9, 11]. For these reasons, an elegant formulation for the exact computation of spherical harmonics coefficients from a constant density polyhedron was developed by Werner [14].

However, it is crucial to note that the literature does not address the problem of uncertainty quantification in the gravity spherical harmonics coefficients arising from an uncertain shape. Any variation of the nominal shape, even when localized, induces variations in the set of all gravity spherical harmonics coefficients and, as a consequence, in the gravity potential and acceleration. Even though Melman et al. [15] addresses the problem of trajectory design and propagation under an uncertain gravity field represented with spherical harmonics using Monte-Carlo simulations, this work does not compute the uncertainty in the spherical harmonics in a rigorous way, as the considered values are taken from Takahashi and Scheeres's work [16]. In this latter paper, gravity characterization of a small body is performed by means of flybys with radiometric and optical measurements, but the orbit determination filter's first guess is not directly deduced from the stochastic shape of the asteroid under study and the a priori filter setting is not thoroughly discussed.

Bercovici et al. [17], a companion work of the present article, investigates the influence of an uncertain shape on the polyhedral gravity model and quantifies the uncertainty in gravity potential, gravity acceleration and gravitational slopes. Moreover, Bercovici and McMahon [18] presents the uncertainties in the inertia parameter of a small body when the shape is considered stochastic and this latter work is related to the uncertainty of the spherical harmonics coefficients of degree 1 and 2.

The present paper provides a fully analytic model to characterize in a linear framework the spherical harmonics coefficients and their uncertainties from a stochastic polyhedral shape up to a generic degree and order. A previous attempt to represent a stochastic small body is carried out by Muinonen [19]. In

this work, the small body radius is modeled as a sum of stochastic spherical harmonics. Unfortunately, this model fails when a concave polyhedron is considered and the uncertainty quantification requires the small body shape to be represented in terms of Muinonen's radius series expansion, which is rather restrictive. On the contrary, in this paper, the shape is represented as a Gaussian variable centered at the nominal polyhedron with a known covariance matrix. The analytical derivations developed therein have multiple applications in the deep space navigation and planetary science fields. As an example, the present analytical model can be used by mission designers to take into account the uncertainty in the polyhedral model deduced from light-curves or radio data while designing the operational orbits. The obtained results can be useful to design trajectories where the uncertain shape has limited effect on the the uncertainty in the gravity acceleration and, as a consequence, on the satellite motion. Moreover, the present model can be used in the estimation process performed during orbit determination. Once the shape has been estimated, the uncertainty can be used to size the a priori uncertainty in order to better process the trajectory arcs. Otherwise, the uncertainties caused by the constant-density stochastic shape could explain the estimation of inhomogeneity in case the spherical harmonics coefficients estimated from navigation data fall within the shape-induced uncertainty range. Finally, the present model provides a valuable and efficient method to compute the spherical harmonics nominal value and the associated uncertainties for orbit determination . An example could be the update of the spherical harmonics coefficients and the computation of the related uncertainty to initialize the orbit determination filter during the approach phase .

2 Notation

The following notations are used in this work:

- Scalar variables are in plain font, as ρ and M
- Vectors are in bold, as $\boldsymbol{r}$ and $\boldsymbol{\Phi}$
- Matrices are between square brackets and in plain font, as $[\Sigma]$
- Vector definition is made with parenthesis, as $\boldsymbol{\xi} = (x,\, y,\, z)^T$

3 The spherical harmonics coefficients derived from a constant density polyhedron

Werner [14] proposes an exact formulation to deduce the spherical harmonics coefficients from a constant density polyhedron. A summary of Werner's work is provided in this section but any reader interested in a more detailed and complete formulation can refer to Reference 14 for implementation details and full derivation of the algorithm.

As spherical harmonics coefficients are directly linked with the gravity field of the body under consideration, their computation relies on the shape of the body and its internal density distribution. When both of these quantities are known, the fully normalized coefficients of degree n and order m, labeled $\bar{C}_{n,m}$ and $\bar{S}_{n,m}$, can be evaluated by computing the following integral under the hypothesis of constant density:

$$\begin{pmatrix} \bar{C}_{n,m} \\ \bar{S}_{n,m} \end{pmatrix} = \rho \iiint_{\text{Body}} \begin{pmatrix} \bar{c}_{n,m} \\ \bar{s}_{n,m} \end{pmatrix} \mathrm{d}x\, \mathrm{d}y\, \mathrm{d}z \tag{1}$$

where ρ is the density of the body. Moreover, the integrands $\bar{c}_{n,m}$ and $\bar{s}_{n,m}$ are special functions to be integrated over the body's shape to evaluate the contribution of the shape on the spherical harmonics functional basis.

In this work, as in Werner's one, the spherical harmonics coefficients and the integrands are organized as follows:

- The coefficients with $m = n$ are called diagonal coefficients
- The coefficients with $m = n - 1$ are called sub-diagonal coefficients

– All the other coefficients, i.e. $m < n-1$, are called vertical coefficients

The first result shown by Werner is the gathering of some relationships to recursively compute the integrands $\bar{c}_{n,m}$ and $\bar{s}_{n,m}$ by starting from some known, also called anchor, conditions.

The diagonal coefficients, viz. $m = n$, are computed from the given formula:

$$\begin{pmatrix} \bar{c}_{n,n} \\ \bar{s}_{n,n} \end{pmatrix} = \frac{2n-1}{a\sqrt{2n(2n+1)}} \begin{bmatrix} x & -y \\ y & x \end{bmatrix} \begin{pmatrix} \bar{c}_{n-1,n-1} \\ \bar{s}_{n-1,n-1} \end{pmatrix} \qquad \text{if } n > 1 \tag{2}$$

where a is the reference radius of the spherical harmonics expansion and $\boldsymbol{\xi} = (x, y, z)$ is a set of Cartesian coordinates whose components are expressed in a predefined orthonormal reference frame.

To start the recursive formulas, the required anchor conditions are:

$$\begin{pmatrix} \bar{c}_{0,0} \\ \bar{s}_{0,0} \end{pmatrix} = \frac{1}{M} \begin{pmatrix} 1 \\ 0 \end{pmatrix} \tag{3}$$

$$\begin{pmatrix} \bar{c}_{1,1} \\ \bar{s}_{1,1} \end{pmatrix} = \frac{1}{M\, a\sqrt{3}} \begin{pmatrix} x \\ y \end{pmatrix} \tag{4}$$

where M is the body mass.

The sub-diagonal coefficients, viz. $m = n-1$, are computed from:

$$\begin{pmatrix} \bar{c}_{n,n-1} \\ \bar{s}_{n,n-1} \end{pmatrix} = \frac{2n-1}{\sqrt{2n+1}} \frac{z}{a} \begin{pmatrix} \bar{c}_{n-1,n-1} \\ \bar{s}_{n-1,n-1} \end{pmatrix} \tag{5}$$

Otherwise, the vertical relationships are:

$$\begin{aligned} \begin{pmatrix} \bar{c}_{n,m} \\ \bar{s}_{n,m} \end{pmatrix} =& (2n-1)\sqrt{\frac{2n-1}{(2n+1)(n+m)(n-m)}} \frac{z}{a} \begin{pmatrix} \bar{c}_{n-1,m} \\ \bar{s}_{n-1,m} \end{pmatrix} + \\ &- \sqrt{\frac{(2n-3)(n+m-1)(n-m-1)}{(2n+1)(n+m)(n-m)}} \left(\frac{r}{a}\right)^2 \begin{pmatrix} \bar{c}_{n-2,m} \\ \bar{s}_{n-2,m} \end{pmatrix} \end{aligned} \tag{6}$$

where $r^2 = x^2 + y^2 + z^2$. It is important to notice that, because of the recursivity of Equations 2 - 6, all the coefficients are directly functions of the body mass M. Moreover, the coefficients are rational functions of the Cartesian coordinates $\boldsymbol{\xi}$ as their computation implies only multiplications and integer powers. As a consequence, the integrands can be expressed as trinomials of the $\boldsymbol{\xi}$ variables.

These quantities must be integrated over an extended body so as to obtain its fully normalized spherical harmonics gravity coefficients of degree n and order m as reported in Equation 1. Moreover, when the integration is performed over a polyhedron, broken up in a collection of tetrahedra, the full integral is equivalent to the summation of the integrals over each tetrahedron.

Let $\mathcal{E} = \{E, \boldsymbol{e}_1, \boldsymbol{e}_2, \boldsymbol{e}_3\}$ be the orthonormal basis local to polyhedron, where E is the basis origin and $\boldsymbol{e}_i$ with $i \in \{1, 2, 3\}$ denotes the ith coordinate unit vector. The set of Cartesian coordinates $\boldsymbol{\xi}$ are

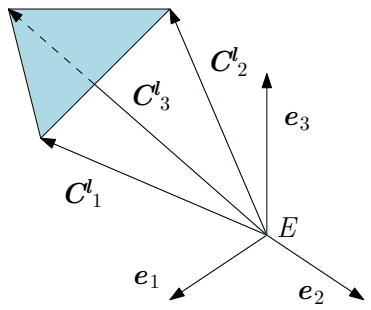

Fig. 1: The bases $\mathcal{E}$ and $\mathcal{T}^l$ for a given tetrahedron.

expressed in the $\mathcal{E}$ basis. Let $\boldsymbol{C}^l{}_i = (x_i,\, y_i,\, z_i)^T$ with $i \in \{1,\, 2,\, 3\}$ denote the coordinates of the ith vertex of the lth facet of the polyhedron expressed in the $\mathcal{E}$ basis. Let $\mathcal{T}^l = \left\{E, \boldsymbol{C}^l{}_1,\, \boldsymbol{C}^l{}_2,\, \boldsymbol{C}^l{}_3\right\}$ be the tetrahedron basis associated with the lth facet. It is important to note that $\mathcal{T}^t$ is not an orthonormal basis. Moreover, let $\boldsymbol{\Xi} = (X,\, Y,\, Z)^T$ denotes the set of coordinates whose components are expressed in the $\mathcal{T}^l$ basis. The two bases are presented in Figure 1.

By applying the change of coordinates $(x,\, y,\, z)^T \mapsto (X,\, Y,\, Z)^T$ between the two previously-defined bases to each tetrahedron

$$\begin{aligned} x\,(X,Y,Z) &= x_1\,X + x_2\,Y + x_3\,Z \\ y\,(X,Y,Z) &= y_1\,X + y_2\,Y + y_3\,Z \\ z\,(X,Y,Z) &= z_1\,X + z_2\,Y + z_3\,Z \end{aligned} \tag{7}$$

the integral can be explicitly computed. The change of coordinates introduced in Equation 7 can be rewritten in a compact form :

$$\boldsymbol{\xi} = \begin{bmatrix} x_1 & x_2 & x_3 \\ y_1 & y_2 & y_3 \\ z_1 & z_2 & z_3 \end{bmatrix} \boldsymbol{\Xi} \tag{8}$$

As the transformation is linear, the integrands remain trinomials of the new variables:

$$\begin{pmatrix} \bar{c}_{n,m} \\ \bar{s}_{n,m} \end{pmatrix} = \sum_{i+j+k=n} \begin{pmatrix} \bar{\alpha}_{ijk} \\ \bar{\beta}_{ijk} \end{pmatrix} X^i\, Y^j\, Z^k \tag{9}$$

where the coefficients $\bar{\alpha}_{ijk}$ and $\bar{\beta}_{ijk}$ are polynomial functions of the vertices coordinates and of the body mass. Their computation relies on the recursive relationships in Equations 2 - 6.

By analytical integration in the $\boldsymbol{\Xi}$ variables, a closed expression of the fully-normalized coefficients is obtained:

$$\begin{pmatrix} \bar{C}_{n,m} \\ \bar{S}_{n,m} \end{pmatrix} = \rho \sum_{\text{tetrahedra}} \frac{\det\left[J\right]}{(n+3)!} \sum_{i+j+k=n} i!j!k! \begin{pmatrix} \bar{\alpha}_{ijk} \\ \bar{\beta}_{ijk} \end{pmatrix} \tag{10}$$

where $[J]$ is the Jacobian of the coordinates transformation given by:

$$[J] = \left[\frac{\partial \boldsymbol{\xi}}{\partial \boldsymbol{\Xi}}\right] = \begin{bmatrix} x_1 & x_2 & x_3 \\ y_1 & y_2 & y_3 \\ z_1 & z_2 & z_3 \end{bmatrix} \tag{11}$$

In conclusion, the cited formulation considers the polyhedron as a collection of tetrahedra and derives the exact integration formula to compute the spherical harmonics coefficients from the tetrahedra's summation. The evaluation of the coefficients $\bar{\alpha}_{ijk}$ and $\bar{\beta}_{ijk}$ must be performed by numerical means as they are computed iteratively. To address this issue, Werner proposes the use of a Truncated Trinomials Algebra (TTA) [14].

4 Mathematical reformulation

The first needed step to quantify the uncertainties due to a stochastic shape on the spherical harmonics coefficients is to formulate the problem in a different fashion. The formulation proposed in the present section has been chosen mainly for two reasons. First, it allows the deduction of derivatives in a straightforward and compact manner by clearly identifying and isolating the components depending on the vertices' coordinates - the volume, the change of coordinates' Jacobian and the coefficients $\bar{\alpha}_{ijk}$ and $\bar{\beta}_{ijk}$. Second, it is well suited for numerical implementation when a TTA is implemented and it avoids round-off errors (see Section 9).

By denoting $[\mathbb{I}_3]$ the 3-dimensional identity matrix and by defining

$$[\Lambda] = \left[X\left[\mathbb{I}_3\right] \mid Y\left[\mathbb{I}_3\right] \mid Z\left[\mathbb{I}_3\right]\right] \tag{12}$$

Equation 7 is rewritten as follows:

$$\boldsymbol{\xi} = [\Lambda]\,\boldsymbol{C}^l \tag{13}$$

where $\boldsymbol{C}^l = \left(\boldsymbol{C}^{l^T}_1\ \boldsymbol{C}^{l^T}_2\ \boldsymbol{C}^{l^T}_3\right)^T$ is the vector containing the coordinates of the tetrahedron vertices, excluding the origin E, with the local numbering. The local numbering i is defined by starting from a vertex of the considered facet and counting counterclockwise by labeling the three vertices with the associated local ID, i.e. 1, 2, or 3. This local numbering is contrasted with the global numbering, which indicates the vertex ID in the complete shape model.

The distance between the origin and the point of interest is expressed by:

$$r^2 = \boldsymbol{\xi}^T\boldsymbol{\xi} = \boldsymbol{C}^{l^T}\,[\Lambda]^T\,[\Lambda]\,\boldsymbol{C}^l \tag{14}$$

The point of interest Cartesian coordinates are related to the local coordinates through

$$x = \boldsymbol{e}_1^T\,[\Lambda]\,\boldsymbol{C}^l \tag{15}$$

$$y = \boldsymbol{e}_2^T\,[\Lambda]\,\boldsymbol{C}^l \tag{16}$$

$$z = \boldsymbol{e}_3^T\,[\Lambda]\,\boldsymbol{C}^l \tag{17}$$

Finally, to get more compact notation and reduce numerical issues (see Section 9), it is useful to define:

$$\bar{\boldsymbol{\phi}}_{n,m} = M\begin{pmatrix}\bar{c}_{n,m}\\ \bar{s}_{n,m}\end{pmatrix} \tag{18}$$

$$\bar{\boldsymbol{\Phi}}_{n,m} = \begin{pmatrix}\bar{C}_{n,m}\\ \bar{S}_{n,m}\end{pmatrix} \tag{19}$$

$$[\mathbb{J}_2] = \begin{bmatrix}0 & -1\\ 1 & 0\end{bmatrix} \tag{20}$$

$$\boldsymbol{\gamma}^{(n,m)}_{ijk} = M\begin{pmatrix}\bar{\alpha}_{ijk}\\ \bar{\beta}_{ijk}\end{pmatrix} \tag{21}$$

$$k_1^{(n,m)} = (2n-1)\sqrt{\frac{2n-1}{(2n+1)(n+m)(n-m)}}\frac{1}{a} \tag{22}$$

$$k_2^{(n,m)} = \sqrt{\frac{(2n-3)(n+m-1)(n-m-1)}{(2n+1)(n+m)(n-m)}}\left(\frac{1}{a}\right)^2 \tag{23}$$

Thanks to the previous definitions, a more compact notation is introduced for the recursive formulas, which are rewritten in the following way:

$$\bar{\boldsymbol{\phi}}_{0,0} = \begin{pmatrix}1\\ 0\end{pmatrix} \tag{24}$$

$$\bar{\boldsymbol{\phi}}_{1,1} = \frac{1}{a\sqrt{3}}\begin{bmatrix}\boldsymbol{e}_1^T\\ \boldsymbol{e}_2^T\end{bmatrix}[\Lambda]\,\boldsymbol{C}^l \tag{25}$$

$$\bar{\boldsymbol{\phi}}_{n,n} = \frac{2n-1}{a\sqrt{2n(2n+1)}}\left([\mathbb{I}_2]\left(\boldsymbol{e}_1^T\,[\Lambda]\,\boldsymbol{C}^l\right) + [\mathbb{J}_2]\left(\boldsymbol{e}_2^T\,[\Lambda]\,\boldsymbol{C}^l\right)\right)\bar{\boldsymbol{\phi}}_{n-1,n-1} \qquad \text{if } n > 1 \tag{26}$$

$$\bar{\boldsymbol{\phi}}_{n,n-1} = \frac{2n-1}{a\sqrt{2n+1}} \left(\boldsymbol{e}_3^T \left[\Lambda\right] \boldsymbol{C}^l\right) \bar{\boldsymbol{\phi}}_{n-1,n-1} \tag{27}$$

$$\bar{\boldsymbol{\phi}}_{n,m} = k_1^{(n,m)} \left(\boldsymbol{e}_3^T \left[\Lambda\right] \boldsymbol{C}^l\right) \bar{\boldsymbol{\phi}}_{n-1,m} - k_2^{(n,m)} \left(\boldsymbol{C}^{l^T} \left[\Lambda\right]^T \left[\Lambda\right] \boldsymbol{C}^l\right) \bar{\boldsymbol{\phi}}_{n-2,m} \tag{28}$$

Moreover, it is useful to define the tetrahedron volume V as a function of the polyhedral vertices:

$$V = \frac{1}{6} \sum_{\text{tetrahedra}} \left(\boldsymbol{C}^l{}_1 \times \boldsymbol{C}^l{}_2\right)^T \boldsymbol{C}^l{}_3 = \frac{1}{6} \sum_{\text{tetrahedra}} \left(\left[\tilde{\boldsymbol{C}}_1^l\right] \boldsymbol{C}^l{}_2\right)^T \boldsymbol{C}^l{}_3 \tag{29}$$

where the tilde operator defines the skew-symmetric matrix associated with the cross product operation [20]. By considering that $M = \rho V$, Equation 10 is rewritten as:

$$\bar{\boldsymbol{\Phi}}_{n,m} = \frac{\rho}{M} \sum_{\text{tetrahedra}} \frac{\det\left[J\right]}{(n+3)!} \sum_{i+j+k=n} i!j!k!\, \boldsymbol{\gamma}_{ijk}^{(n,m)} = \frac{1}{V} \sum_{\text{tetrahedra}} \bar{\boldsymbol{\Phi}}_{n,m}^t \tag{30}$$

where $\bar{\boldsymbol{\Phi}}_{n,m}^t$ is the contribution given to the spherical harmonics coefficients $\bar{\boldsymbol{\Phi}}_{n,m}$ of the tetrahedron t.

It is important to notice in Equation 30 that the vertices contributions have been isolated in three different terms: the volume, the transformation Jacobian and the coefficients $\boldsymbol{\gamma}_{ijk}^{(n,m)}$. This isolated representation allows the first variation to be taken straightforwardly.

5 First variations

5.1 First variation of the recursive formulas

To quantify the variation in the spherical harmonics coefficients given by a variation in the vertices positions, the recursive formulas must be considered first. By computing the first variation of Equations 24-28 relative to the vertex coordinates, the following relations are deduced:

$$\delta\bar{\boldsymbol{\phi}}_{0,0} = \begin{pmatrix} 0 \\ 0 \end{pmatrix} \tag{31}$$

$$\delta\bar{\boldsymbol{\phi}}_{1,1} = \frac{1}{a\sqrt{3}} \begin{bmatrix} \boldsymbol{e}_1^T \\ \boldsymbol{e}_2^T \end{bmatrix} \left[\Lambda\right] \left[\mathbb{I}_9\right] \delta\boldsymbol{C}^l \tag{32}$$

Moreover:

$$\begin{aligned} \delta\bar{\boldsymbol{\phi}}_{n,n} =& \frac{2n-1}{a\sqrt{2n(2n+1)}} \left(\left(\left[\mathbb{I}_2\right] \boldsymbol{\phi}_{n-1,n-1} \boldsymbol{e}_1^T \left[\Lambda\right] + \left[\mathbb{J}_2\right] \boldsymbol{\phi}_{n-1,n-1} \boldsymbol{e}_2^T \left[\Lambda\right]\right) \delta\boldsymbol{C}^l + \right. \\ & \left. + \left(\left[\mathbb{I}_2\right] \left(\boldsymbol{e}_1^T \left[\Lambda\right] \boldsymbol{C}^l\right) + \left[\mathbb{J}_2\right] \left(\boldsymbol{e}_2^T \left[\Lambda\right] \boldsymbol{C}^l\right)\right) \delta\bar{\boldsymbol{\phi}}_{n-1,n-1}\right) = \\ =& \frac{2n-1}{a\sqrt{2n(2n+1)}} \left(\left[\Upsilon\right] \delta\boldsymbol{C}^l + \left[\Psi\right] \delta\bar{\boldsymbol{\phi}}_{n-1,n-1}\right) \end{aligned} \tag{33}$$

where $\left[\Upsilon\right]$ and $\left[\Psi\right]$ are defined as:

$$\left[\Upsilon\right] = \left(\left[\mathbb{I}_2\right] \boldsymbol{\phi}_{n-1,n-1} \boldsymbol{e}_1^T \left[\Lambda\right] + \left[\mathbb{J}_2\right] \boldsymbol{\phi}_{n-1,n-1} \boldsymbol{e}_2^T \left[\Lambda\right]\right) \tag{34}$$

$$\left[\Psi\right] = \left(\left[\mathbb{I}_2\right] \left(\boldsymbol{e}_1^T \left[\Lambda\right] \boldsymbol{C}^l\right) + \left[\mathbb{J}_2\right] \left(\boldsymbol{e}_2^T \left[\Lambda\right] \boldsymbol{C}^l\right)\right) \tag{35}$$

$$\delta\bar{\boldsymbol{\phi}}_{n,n-1} = \frac{2n-1}{a\sqrt{2n+1}} \left(\bar{\boldsymbol{\phi}}_{n-1,n-1} \boldsymbol{e}_3^T \left[\Lambda\right] \delta\boldsymbol{C}^l + \left(\boldsymbol{e}_3^T \left[\Lambda\right] \boldsymbol{C}^l\right) \delta\bar{\boldsymbol{\phi}}_{n-1,n-1}\right) \tag{36}$$

$$\begin{aligned} \delta\bar{\boldsymbol{\phi}}_{n,m} = k_1^{(n,m)} & \left(\bar{\boldsymbol{\phi}}_{n-1,m} \boldsymbol{e}_3^T \left[\Lambda\right] \delta\boldsymbol{C}^l + \left(\boldsymbol{e}_3^T \left[\Lambda\right] \boldsymbol{C}^l\right) \delta\bar{\boldsymbol{\phi}}_{n-1,m}\right) + \\ & - k_2^{(n,m)} \left(2\bar{\boldsymbol{\phi}}_{n-2,m} \boldsymbol{C}^{l^T} \left[\Lambda\right]^T \left[\Lambda\right] \delta\boldsymbol{C}^l + \left(\boldsymbol{C}^{l^T} \left[\Lambda\right]^T \left[\Lambda\right] \boldsymbol{C}^l\right) \delta\bar{\boldsymbol{\phi}}_{n-2,m}\right) \end{aligned} \tag{37}$$

5.2 First variation of the global formula

Analogously, the variation of the global formula is computed:

$$\delta\bar{\boldsymbol{\Phi}}_{n,m} = \frac{1}{V}\left(\sum_{\text{tetrahedra}} \delta\bar{\boldsymbol{\Phi}}^t_{n,m} - \frac{1}{V}\left(\sum_{\text{tetrahedra}} \bar{\boldsymbol{\Phi}}^t_{n,m}\right)\delta V\right) = \frac{1}{V}\left(\sum_{\text{tetrahedra}} \delta\bar{\boldsymbol{\Phi}}^t_{n,m} - \bar{\boldsymbol{\Phi}}_{n,m}\delta V\right) \tag{38}$$

$$\delta\bar{\boldsymbol{\Phi}}^t_{n,m} = \frac{1}{(n+3)!}\left(\det[J]\sum_{i+j+k=n} i!j!k!\;\delta\boldsymbol{\gamma}^{(n,m)}_{ijk} + \left(\sum_{i+j+k=n} i!j!k!\;\boldsymbol{\gamma}^{(n,m)}_{ijk}\right)\delta(\det[J])\right) \tag{39}$$

where, by using the fact that the determinant is the signed volume:

$$\delta(\det[J]) = \begin{pmatrix} \left[\tilde{\boldsymbol{C}}^l_2\right]\boldsymbol{C}^l{}_3 \\ \left[\tilde{\boldsymbol{C}}^l_3\right]\boldsymbol{C}^l{}_1 \\ \left[\tilde{\boldsymbol{C}}^l_1\right]\boldsymbol{C}^l{}_2 \end{pmatrix}^T \delta\boldsymbol{C}^l \tag{40}$$

6 From local to global numbering: a summary of the equations

In this section the mapping from the local to the global numbering is presented and the full set of equations is reported for the sake of completeness.

The reader has probably remarked that the analytical derivation has been performed by using the local numbering of the indices and the variational formulation always considers a local representation of the tetrahedron facet. Nevertheless, the aim of the present work is to find the uncertainty in the spherical harmonics coefficients relative to a variation in the overall shape. To address this need, an assembly step must be added in the formulation to express the formulas from the local to the global numbering. This is performed by defining an assembly matrix $\left[K^t_{g\to l}\right]$ that links the indices of the global representation to the local representation as in the Finite Element Method [21].

$$\boldsymbol{C}^l = \left[K^t_{g\to l}\right]\boldsymbol{C} \qquad\qquad \delta\boldsymbol{C}^l = \left[K^t_{g\to l}\right]\delta\boldsymbol{C} \tag{41}$$

where $\boldsymbol{C}$ is the list of all the vertices composing the tetrahedron.

The assembly matrix is a useful tool to easily convert from the local numbering to the full list of vertices composing the polyhedron. By substituting Equation 41 into the equations deduced from the previous variational analysis, the contribution of a single tetrahedron to the partial derivatives with respect to the vertices list is computed:

$$\left[\frac{\partial\bar{\phi}_{0,0}}{\partial\boldsymbol{C}}\right] = [0_{2\times 9}]\left[K^t_{g\to l}\right] \tag{42}$$

$$\left[\frac{\partial\bar{\phi}_{1,1}}{\partial\boldsymbol{C}}\right] = \frac{1}{a\sqrt{3}}\begin{bmatrix}\boldsymbol{e}_1^T \\ \boldsymbol{e}_2^T\end{bmatrix}[\Lambda]\left[K^t_{g\to l}\right] \tag{43}$$

$$\left[\frac{\partial\bar{\phi}_{n,n}}{\partial\boldsymbol{C}}\right] = \frac{2n-1}{a\sqrt{2n(2n+1)}}\left([\Upsilon]\left[K^t_{g\to l}\right] + [\Psi]\left[\frac{\partial\bar{\phi}_{n-1,n-1}}{\partial\boldsymbol{C}}\right]\right) \tag{44}$$

$$\left[\frac{\partial\bar{\phi}_{n,n-1}}{\partial\boldsymbol{C}}\right] = \frac{2n-1}{a\sqrt{2n+1}}\left(\bar{\phi}_{n-1,n-1}\boldsymbol{e}_3^T[\Lambda]\left[K^t_{g\to l}\right] + \left(\boldsymbol{e}_3^T[\Lambda]\boldsymbol{C}^l\right)\left[\frac{\partial\bar{\phi}_{n-1,n-1}}{\partial\boldsymbol{C}}\right]\right) \tag{45}$$

$$\left[\frac{\partial \bar{\phi}_{n,m}}{\partial \boldsymbol{C}}\right] = k_1^{(n,m)} \left(\bar{\phi}_{n-1,m} \boldsymbol{e}_3^T \left[\Lambda\right] \left[K_{g\to l}^t\right] + \left(\boldsymbol{e}_3^T \left[\Lambda\right] \boldsymbol{C}^l\right) \left[\frac{\partial \bar{\phi}_{n-1,m}}{\partial \boldsymbol{C}}\right]\right) + \\ - k_2^{(n,m)} \left(2\bar{\phi}_{n-2,m} {\boldsymbol{C}^l}^T \left[\Lambda\right]^T \left[\Lambda\right] \left[K_{g\to l}^t\right] + \left({\boldsymbol{C}^l}^T \left[\Lambda\right]^T \left[\Lambda\right] \boldsymbol{C}^l\right) \left[\frac{\partial \bar{\phi}_{n-2,m}}{\partial \boldsymbol{C}}\right]\right) \quad (46)$$

$$\left[\frac{\partial \det\left[J\right]}{\partial \boldsymbol{C}}\right] = \begin{pmatrix} \left[\tilde{\boldsymbol{C}}_2^l\right] {\boldsymbol{C}^l}_3 \\ \left[\tilde{\boldsymbol{C}}_3^l\right] {\boldsymbol{C}^l}_1 \\ \left[\tilde{\boldsymbol{C}}_1^l\right] {\boldsymbol{C}^l}_2 \end{pmatrix}^T \left[K_{g\to l}^t\right] \quad (47)$$

$$\left[\frac{\partial \bar{\boldsymbol{\Phi}}_{n,m}^t}{\partial \boldsymbol{C}}\right] = \frac{1}{(n+3)!} \left(\det\left[J\right] \sum_{i+j+k=n} i!j!k! \left[\frac{\partial \boldsymbol{\gamma}_{ijk}^{(n,m)}}{\partial \boldsymbol{C}}\right] + \left(\sum_{i+j+k=n} i!j!k!\, \boldsymbol{\gamma}_{ijk}^{(n,m)}\right) \left[\frac{\partial \det\left[J\right]}{\partial \boldsymbol{C}}\right]\right) \quad (48)$$

where the matrix $\left[\frac{\partial \boldsymbol{\gamma}_{ijk}^{(n,m)}}{\partial \boldsymbol{C}}\right]$ is computed thanks to the TTA as it is expounded in Section 9.

Finally, the partial derivatives of the fully-normalized coefficients of degree n and order m with respect to the overall shape are expressed as follows:

$$\left[\frac{\partial \bar{\boldsymbol{\Phi}}_{n,m}}{\partial \boldsymbol{C}}\right] = \frac{1}{V} \left(\sum_{\text{tetrahedra}} \left[\frac{\partial \bar{\boldsymbol{\Phi}}_{n,m}^t}{\partial \boldsymbol{C}}\right] - \bar{\boldsymbol{\Phi}}_{n,m} \left[\frac{\partial V}{\partial \boldsymbol{C}}\right]\right) \quad (49)$$

where:

$$\left[\frac{\partial V}{\partial \boldsymbol{C}}\right] = \frac{1}{6} \sum_{\text{tetrahedra}} \begin{pmatrix} \left[\tilde{\boldsymbol{C}}_2^l\right] {\boldsymbol{C}^l}_3 \\ \left[\tilde{\boldsymbol{C}}_3^l\right] {\boldsymbol{C}^l}_1 \\ \left[\tilde{\boldsymbol{C}}_1^l\right] {\boldsymbol{C}^l}_2 \end{pmatrix}^T \left[K_{g\to l}^t\right] \quad (50)$$

Furthermore, in order to have a compact notation, the following definitions are introduced:

$$\bar{\boldsymbol{\Phi}} = \begin{pmatrix} \bar{\boldsymbol{\Phi}}_{0,0} \\ \bar{\boldsymbol{\Phi}}_{1,0} \\ \bar{\boldsymbol{\Phi}}_{1,1} \\ \vdots \\ \bar{\boldsymbol{\Phi}}_{N,N-1} \\ \bar{\boldsymbol{\Phi}}_{N,N} \end{pmatrix} \qquad \bar{\boldsymbol{\Phi}}^t = \begin{pmatrix} \bar{\boldsymbol{\Phi}}_{0,0}^t \\ \bar{\boldsymbol{\Phi}}_{1,0}^t \\ \bar{\boldsymbol{\Phi}}_{1,1}^t \\ \vdots \\ \bar{\boldsymbol{\Phi}}_{N,N-1}^t \\ \bar{\boldsymbol{\Phi}}_{N,N}^t \end{pmatrix} \qquad \bar{\boldsymbol{\Gamma}}_{ijk} = \begin{pmatrix} \bar{\boldsymbol{\gamma}}_{ijk}^{0,0} \\ \bar{\boldsymbol{\gamma}}_{ijk}^{1,0} \\ \bar{\boldsymbol{\gamma}}_{ijk}^{1,1} \\ \vdots \\ \bar{\boldsymbol{\gamma}}_{ijk}^{N,N-1} \\ \bar{\boldsymbol{\gamma}}_{ijk}^{N,N} \end{pmatrix} \quad (51)$$

Finally:

$$\left[\frac{\partial \bar{\boldsymbol{\Phi}}}{\partial \boldsymbol{C}}\right] = \frac{1}{V} \left(\sum_{\text{tetrahedra}} \left[\frac{\partial \bar{\boldsymbol{\Phi}}^t}{\partial \boldsymbol{C}}\right] - \bar{\boldsymbol{\Phi}} \left[\frac{\partial V}{\partial \boldsymbol{C}}\right]\right) = \frac{1}{V} \left(\sum_{\text{tetrahedra}} \frac{1}{(n+3)!} \left(\det\left[J\right] \sum_{i+j+k=\nu} i!j!k! \left[\frac{\partial \bar{\boldsymbol{\Gamma}}_{ijk}}{\partial \boldsymbol{C}}\right] + \right.\right. \\ \left.\left. + \left(\sum_{i+j+k=\nu} i!j!k!\, \bar{\boldsymbol{\Gamma}}_{ijk}\right) \left[\frac{\partial \det\left[J\right]}{\partial \boldsymbol{C}}\right]\right) - \bar{\boldsymbol{\Phi}} \left[\frac{\partial V}{\partial \boldsymbol{C}}\right]\right) \quad (52)$$

where ν is a variable that changes according to the position in the vector $\bar{\boldsymbol{\Phi}}$ of each spherical harmonics coefficient $\bar{\boldsymbol{\Phi}}_{n,m}$. The ν variable is needed because $i+j+k$ must be equal to the degree n of the considered spherical harmonics coefficient $\bar{\boldsymbol{\Phi}}_{n,m}$. As the degree of the spherical harmonics coefficients changes with the position in the vector $\bar{\boldsymbol{\Phi}}$, the ν variable changes accordingly.

The derivative computation depends on three main factors: the shape, the distribution of the points (or equivalently the shape of each single tetrahedron), and the spherical harmonics coefficients (which depend on the shape and density). These quantities are intertwined for a general shape like a polyhedron and, as a consequence, it is hard to quantify which is the leading contribution in Equation 52 and the relative importance of each term.

7 Uncertainty quantification

7.1 Uncertainty in the spherical harmonics coefficients

In this section the spherical harmonics coefficients uncertainties are deduced from the previous variational analysis. If the first variation is considered as a stochastic variable, the uncertainty quantification, in a linear framework, can be performed.

In the linear framework, a Gaussian probability density function (PDF) remains Gaussian and, as a consequence, the PDF can be characterized by the first two momenta, the mean and the covariance. The mean of the output PDF is the evaluation of the non-linear function, in this case the function that compute the spherical harmonics coefficients from the polyhedron points $\bar{\boldsymbol{\Phi}} = g(\boldsymbol{C})$, at the nominal value of the linearization. To characterize the second stochastic moment of the output function, the linear framework prescribes that the uncertainty - namely, the covariance matrix - computation is based on the first order derivative of the non-linear function with respect to the input parameters.

As a consequence, by using the computed partial derivatives with respect to the global components of the polyhedron vertices, the uncertainty associated with the spherical harmonics coefficients is computed:

$$[P_{\bar{\boldsymbol{\Phi}}}] = \mathbb{E}\left\{\delta\bar{\boldsymbol{\Phi}}\,\delta\bar{\boldsymbol{\Phi}}^T\right\} = \left[\frac{\partial\bar{\boldsymbol{\Phi}}}{\partial\boldsymbol{C}}\right][P_{\boldsymbol{C}}]\left[\frac{\partial\bar{\boldsymbol{\Phi}}}{\partial\boldsymbol{C}}\right]^T \tag{53}$$

where $[P_{\boldsymbol{C}}]$ is the covariance of the points composing the polyhedron.

7.2 Uncertainty in the gravity potential

A straightforward application of the characterization of the uncertainty in the spherical harmonics coefficients is the uncertainty quantification of the corresponding potential.

The gravity potential expressed in spherical harmonics is recalled [22]:

$$U(\boldsymbol{r}) = \frac{GM}{r}\sum_{n=0}^{N}\sum_{m=0}^{n}\left(\frac{a}{r}\right)^n \bar{P}_{n,m}(\sin\varphi)\left(\bar{C}_{n,m}\cos m\lambda + \bar{S}_{n,m}\sin m\lambda\right) \tag{54}$$

where G is the universal gravity constant, $\bar{P}_{n,m}$ is the associated Legendre function of degree n and order m (see Appendix A for definition and recursive formulas), (φ,λ) are the latitude and longitude respectively.

By defining:

$$\bar{\boldsymbol{\Pi}} = \begin{pmatrix} \bar{P}_{0,0} \\ \bar{P}_{0,0} \\ \left(\frac{a}{r}\right) \bar{P}_{1,0} \cos\lambda \\ \left(\frac{a}{r}\right) \bar{P}_{1,0} \sin\lambda \\ \left(\frac{a}{r}\right)^2 \bar{P}_{2,0} \cos 2\lambda \\ \vdots \\ \left(\frac{a}{r}\right)^N \bar{P}_{N,N} \cos N\lambda \\ \left(\frac{a}{r}\right)^N \bar{P}_{N,N} \sin N\lambda \end{pmatrix} \tag{55}$$

The gravitation potential takes a more compact form:

$$U = \frac{G\rho V}{r} \bar{\boldsymbol{\Pi}}^T \bar{\boldsymbol{\Phi}} \tag{56}$$

The first variation is then computed:

$$\delta U(\boldsymbol{r}) = \frac{G\rho}{r} \begin{bmatrix} \bar{\boldsymbol{\Pi}}^T \bar{\boldsymbol{\Phi}} & V \boldsymbol{\Pi}^T \end{bmatrix} \begin{pmatrix} \delta V \\ \delta \bar{\boldsymbol{\Phi}} \end{pmatrix} = \frac{G\rho}{r} \begin{bmatrix} \bar{\boldsymbol{\Pi}}^T \bar{\boldsymbol{\Phi}} & V \boldsymbol{\Pi}^T \end{bmatrix} \begin{pmatrix} \dfrac{\partial V}{\partial \boldsymbol{C}} \\ \dfrac{\partial \bar{\boldsymbol{\Phi}}}{\partial \boldsymbol{C}} \end{pmatrix} \delta \boldsymbol{C} = [\mathcal{U}]\, \delta \boldsymbol{C} \tag{57}$$

where $[\mathcal{U}]$ is the linear mapping between the variation of the potential and the variation of vertices coordinates. Its definition is given by Equation 57 and it must be remembered that $[\mathcal{U}]$ is a function of the distance to the polyhedron origin.

By considering the variation with respect to the nominal value as a stochastic variable:matrix mapping the variation between

$$P_U(\boldsymbol{r}) = \mathbb{E}\left\{\delta U\, \delta U^T\right\} = [\mathcal{U}]\, \mathbb{E}\left\{\delta \boldsymbol{C} \delta \boldsymbol{C}^T\right\} [\mathcal{U}]^T = [\mathcal{U}]\, P_{\boldsymbol{C}}\, [\mathcal{U}]^T \tag{58}$$

7.3 Uncertainty in the gravity acceleration

Analogously, the uncertainty in gravity acceleration with a spherical harmonics representation can be computed directly from the previously given formulas. It must be noted that several implementations have been proposed to compute the gravity acceleration from the spherical harmonics potential [23–26]. The one proposed by Gottlieb is used in this work to deduce the uncertainty in the gravity acceleration as it has no singularity at the pole, it is expressed in Cartesian coordinates and it uses fully-normalized coefficients [24, 26]. The formulation of the acceleration presented hereunder also considers the first degree spherical harmonics functions as the Gottlieb's work makes the hypothesis to have a reference frame centered in the center of mass of the considered body, viz. $\bar{\boldsymbol{\Phi}}_{1,0} = \bar{\boldsymbol{\Phi}}_{1,1} = \boldsymbol{0}$. This statement is not verified when the shape is stochastic as any variation of the shape implies a movement of the center of mass and a variation of $\bar{\boldsymbol{\Phi}}_{1,0}$ and $\bar{\boldsymbol{\Phi}}_{1,1}$ as the two quantities are coupled [5, 27].

The acceleration is:

$$\boldsymbol{a}(\boldsymbol{r}) = -\frac{GM}{r^2}\sum_{n=0}^{N}\sum_{m=0}^{n}\left(\sqrt{\frac{(n-m)(2-\delta_{m\,0})(n+m+1)}{2}}B_{n,m}\left(\frac{a}{r}\right)^n\frac{\bar{P}_n^{m+1}}{r^m}\frac{\boldsymbol{e}_3^T\boldsymbol{r}}{r}\frac{\boldsymbol{r}}{r}+\right.$$
$$+\left(\frac{a}{r}\right)^n\frac{\bar{P}_n^m}{r^m}(n+m+1)\,B_{n,m}\frac{\boldsymbol{r}}{r}-\sqrt{\frac{(n-m)(2-\delta_{m\,0})(n+m+1)}{2}}\left(\frac{a}{r}\right)^n\frac{\bar{P}_n^{m+1}}{r^m}B_{n,m}\boldsymbol{e}_3+$$
$$\left.-\frac{\bar{P}_n^m}{r^{m-1}}m\begin{pmatrix}\bar{C}_{n,m}C_{m-1}+\bar{S}_{n,m}S_{m-1}\\-\bar{C}_{n,m}S_{m-1}+\bar{S}_{n,m}C_{m-1}\\0\end{pmatrix}\right) \tag{59}$$

where $\bar{P}_n^m$ is the mth derivative of the fully normalized Legendre polynomial of degree n, also known as derivative Legendre function (see Appendix A for definition and recursive formulas), δ_{0m} is the Kronecker function and C_m, S_m and $B_{n,m}$ are defined as follows:

$$C_m = \varrho^m\cos m\lambda \tag{60}$$

$$S_m = \varrho^m\sin m\lambda \tag{61}$$

$$B_{n,m} = \bar{C}_{n,m}C_m + \bar{S}_{n,m}S_m \tag{62}$$

where $\varrho = \sqrt{x^2+y^2}$. The coefficients C_m and S_m are defined recursively [24]:

$$C_0 = 1 \qquad S_0 = 0 \tag{63}$$

$$C_1 = \frac{\boldsymbol{r}\cdot\boldsymbol{e}_1}{\boldsymbol{r}} \qquad S_1 = \frac{\boldsymbol{r}\cdot\boldsymbol{e}_2}{\boldsymbol{r}} \tag{64}$$

$$C_m = C_1\,C_{m-1} - S_1\,S_{m-1} \qquad S_1 = S_1\,C_{m-1} + C_1\,S_{m-1} \tag{65}$$

In order to have a more compact notation, it is useful to define:

$$\boldsymbol{\varsigma}_m = \begin{pmatrix}C_m\\S_m\end{pmatrix} \tag{66}$$

$$[\check{\varsigma}_m] = \begin{bmatrix}C_m & -S_m\\S_m & C_m\end{bmatrix} \tag{67}$$

As a consequence:

$$\boldsymbol{\varsigma}_0 = \begin{pmatrix}1\\0\end{pmatrix} \qquad \boldsymbol{\varsigma}_1 = \begin{pmatrix}\dfrac{\boldsymbol{r}^T\boldsymbol{e}_1}{\boldsymbol{r}}\\[2ex]\dfrac{\boldsymbol{r}^T\boldsymbol{e}_2}{\boldsymbol{r}}\end{pmatrix} \tag{68}$$

$$\boldsymbol{\varsigma}_m = [\check{\varsigma}_1]\,\boldsymbol{\varsigma}_{m-1} \qquad \text{if m} > 1 \tag{69}$$

Moreover, the acceleration is rewritten as:

$$\boldsymbol{a} = -\frac{GM}{r^2}\sum_{n=0}^{N}\sum_{m=0}^{n}\left(\sqrt{\frac{(n-m)(2-\delta_{m\,0})(n+m+1)}{2}}\left(\frac{a}{r}\right)^n\frac{\bar{P}_n^{m+1}}{r^m}\frac{\boldsymbol{e}_3^T\boldsymbol{r}}{r}\frac{\boldsymbol{r}}{r}\boldsymbol{\varsigma}_m^T+\right.$$
$$+\left(\frac{a}{r}\right)^n\frac{\bar{P}_n^m}{r^m}(n+m+1)\,\frac{\boldsymbol{r}}{r}\boldsymbol{\varsigma}_m^T-\sqrt{\frac{(n-m)(2-\delta_{m\,0})(n+m+1)}{2}}\left(\frac{a}{r}\right)^n\frac{\bar{P}_n^{m+1}}{r^m}\boldsymbol{e}_3\boldsymbol{\varsigma}_m^T+$$
$$\left.-\frac{\bar{P}_n^m}{r^{m-1}}m\,[\boldsymbol{e}_1\,\boldsymbol{e}_2]\,[\check{\varsigma}_{m-1}]^T\right)\bar{\boldsymbol{\Phi}}_{n,m} \tag{70}$$

As a consequence:

$$\boldsymbol{a} = -\frac{GM}{r^2} \sum_{n=0}^{N} \sum_{m=0}^{n} [\sigma_{n,m}] \, \bar{\boldsymbol{\Phi}}_{n,m} \tag{71}$$

Or:

$$\boldsymbol{a} = -\frac{G\rho V}{r^2} [\Sigma] \, \bar{\boldsymbol{\Phi}} \tag{72}$$

with

$$\Sigma = \begin{bmatrix} \sigma_{0,0} & \sigma_{1,0} & \sigma_{1,1} & \cdots & \sigma_{N,N} \end{bmatrix} \tag{73}$$

By variational analysis, the uncertainty in the acceleration is gathered:

$$\delta \boldsymbol{a}(\boldsymbol{r}) = -\frac{G\rho}{r^2} \begin{bmatrix} [\Sigma] \, \bar{\boldsymbol{\Phi}} & V[\Sigma] \end{bmatrix} \begin{pmatrix} \dfrac{\partial V}{\partial \boldsymbol{C}} \\ \dfrac{\partial \bar{\boldsymbol{\Phi}}}{\partial \boldsymbol{C}} \end{pmatrix} \delta \boldsymbol{C} = [\mathcal{A}] \, \delta \boldsymbol{C} \tag{74}$$

where $[\mathcal{A}]$ is the linear mapping between the variation of the gravity acceleration and the variation of vertices coordinates. Its definition is given by Equation 74 and it must be remembered that $[\mathcal{A}]$ is a function of the distance to the polyhedron origin. Finally:

$$[P_{\boldsymbol{a}}](\boldsymbol{r}) = \mathbb{E}\left\{\delta \boldsymbol{a} \, \delta \boldsymbol{a}^T\right\} = [\mathcal{A}] \, \mathbb{E}\left\{\delta \boldsymbol{C} \delta \boldsymbol{C}^T\right\} [\mathcal{A}]^T = [\mathcal{A}] \, [P_{\boldsymbol{C}}] \, [\mathcal{A}]^T \tag{75}$$

8 The covariance $[P_{\boldsymbol{C}}]$

In this section polyhedron covariance is presented and the needed regularization to address the problem of sampling the PDF in order to generate the Monte-Carlo samples.

It must be noticed that the present work is completely independent with respect to the chosen covariance matrix $[P_{\boldsymbol{C}}]$ as the uncertainty quantification is performed in a linear framework. Nevertheless, it is important to introduce the covariance matrix that has been used for this study as it allows the reader to understand and interpret thoroughly the presented results.

The idea behind the construction of the vertices coordinate covariance matrix is based on the idea that each vertex has its own standard deviation σ and, due to its movement, it perturbs the close vertices within a given perturbation length l [18, 28]. As a consequence, the covariance of the stochastic shape has the following form:

$$[P_{\boldsymbol{C}}]_{ii} = \mathbb{E}\left\{\delta \boldsymbol{C}_i \delta \boldsymbol{C}_i^T\right\} = \sigma^2 \hat{\boldsymbol{r}}_i \hat{\boldsymbol{r}}_i^T \tag{76}$$

where σ is the variance of the considered vertex and $\hat{\boldsymbol{r}}_i$ is the radial unity vector between the center of mass of the considered shape and the ith vertex. Moreover:

$$[P_{\boldsymbol{C}}]_{ij} = \mathbb{E}\left\{\delta \boldsymbol{C}_i \delta \boldsymbol{C}_j^T\right\} = \sigma^2 \hat{\boldsymbol{r}}_i \hat{\boldsymbol{r}}_j^T \exp\left\{-\frac{(\boldsymbol{C}_i - \boldsymbol{C}_j)^T (\boldsymbol{C}_i - \boldsymbol{C}_j)}{2l^2}\right\} \tag{77}$$

where l is a relaxation factor.

From a numerical point of view the previously-defined matrix is ill-conditioned. When the shape of the asteroid (16) Psyche is considered, $\sigma = 3$ km and $l = 75$ km the matrix condition number is $\sim 10^{24}$. This ill-conditioning is problematic when the Gaussian PDF must be sampled in order to obtain the Monte-Carlo samples to validate the proposed linearized approach. In particular, the Cholesky decomposition cannot provide good results when the matrix is highly ill-conditioned as in the previous example. To avoid this problem, a regularization algorithm has been developed and implemented.

As the matrix is squared, a spectral decomposition, which is equivalent to the Singular Value Decomposition for real squared matrices, of the covariance matrix can be computed as follows:

$$[P_{\boldsymbol{C}}] = [W]\,[D]\,[W]^{-1} \tag{78}$$

The matrix is positive definite by construction, as the reader can deduce from Equations 76 and 77. Therefore any negative eigenvalue present in the matrix $[D]$ is caused by numerical ill-conditioning of the covariance matrix. Moreover, as the matrix $[W]$ is an orthogonal matrix because of the properties of the spectral decomposition, it is recalled that:

$$[P_{\boldsymbol{C}}] = [W]\left[\sqrt{D}\right][W]^{-1}[W]\left[\sqrt{D}\right][W]^{-1} = [W]\left[\sqrt{D}\right]\left[\sqrt{D}\right][W]^{-1} \tag{79}$$

where the square root of $[D]$ is defined as $\left[\sqrt{D}\right]_{ii} = \sqrt{[D]_{ii}}$. The regularization procedure operates by setting all negative eigenvalues to zero and it produces a regularized eigenvalue matrix $[D']$ defined as:

$$\left[\sqrt{D'}\right]_{ii} = \begin{cases} 0 & \text{if } [D]_{ii} \leq 0 \\ \sqrt{[D]_{ii}} & \text{otherwise} \end{cases} \tag{80}$$

In a second step, a regularized form of the covariance matrix is computed:

$$[P'_{\boldsymbol{C}}] = [W]\left[\sqrt{D'}\right]\left[\sqrt{D'}\right][W]^{-1} \tag{81}$$

This last step is needed to compare the results between the Monte-Carlo simulation and the proposed linearized approach.

In the following sections the notation $[P_{\boldsymbol{C}}]$ is used even though the regularization has been performed for all the simulations.

9 Implementation

In this section the implementation procedure specific to the proposed model is described as some careful precautions and dedicated techniques must be used.

Firstly, as described in Werner's paper, a TTA has been implemented in order to compute recursively compute the vector $\bar{\boldsymbol{\Gamma}}_{ijk}$ and the matrix $\left[\frac{\partial \bar{\boldsymbol{\Gamma}}_{ijk}}{\partial \boldsymbol{C}}\right]$ for all the tetrahedra. Moreover, as the proposed TTA works in a scalar framework, the algebra has been extended to the matrix case by carefully verifying matrix properties and scalar ones. Interested readers can refer to Reference 29 for a general framework of truncated polynomial algebras. The operations implemented in the algebra are:

1. Addition
2. Subtraction
3. Transposition of the matrix coefficients
4. Multiplication with a scalar or a matrix
5. Multiplication with another truncated trinomial
6. Integration of the trinomial with respect to the three variables

Secondly, a parallelization of the library is a crucial issue in order to speed up computations. The multiplication with respect to another truncated trinomial is a time consuming operation as all the elements of the trinomial whose final degree is smaller than the trinomial degree must be considered for this operation. Moreover, the computation of $\bar{\boldsymbol{\Gamma}}_{ijk}$ and $\left[\frac{\partial \bar{\boldsymbol{\Gamma}}_{ijk}}{\partial \boldsymbol{C}}\right]$ is performed on one tetrahedron before having its contribution summed up with the other tetrahedra in order to compute the final spherical harmonics coefficients for the overall shape. It must be noted that each tetrahedron is independent from the others. From these considerations, parallelization of the code could be performed at different

levels, i.e. when performing the trinomial multiplication or when computing the contribution of each tetrahedron. The parallelization has been implemented at the highest level possible, i.e. computing each tetrahedron contribution, as this is the most independent series of operation in the presented algorithm. This choice is made to limit access to the central memory where global data is stored and, as a consequence, reduces the interaction among the different workers and their communication with the central memory.

Third, it is very important to avoid numerical round-off errors due to underflow and overflow. Two approaches are considered in the present work: the choice of distance unit and an intelligent reformulation of the problem in Section 4. On the one hand, the definition of $\bar{\boldsymbol{\phi}}_{n,m}$ in Equation 18 includes the mass in order to avoid the division of the computed integrands by a quite large number, thus avoiding the underflow problem. On the other hand, the choice of distance unit is a crucial factor. By looking at Equations 52, 58 and 75, it must be noticed that constants with very different magnitudes are multiplied and, as a consequence, underflow or overflow could be encountered during computations. For example, if the spherical harmonics coefficients of the asteroid (16) Psyche are computed, distance unit must be set in kilometers as the reference radius is 140 km so as to avoid underflow.

Validation has been performed on the code in order to ensure the correctness of the expounded results. Different procedures have been implemented and can be summarized as follows:

- The TTA has been validated by unitary and validation tests. In particular the properties, such as commutativity, distributivity and associativity, of the algebra operations have been verified.
- The correct computation of the spherical harmonics coefficients has been verified by known examples in the literature. The coefficients computed from the shape of the asteroid (433) Eros available in the Planetary Data System - Small Body Node [30] have been compared with the one available in Reference 11 and the results agree at the 3rd decimal maximum. Moreover, the spherical harmonics coefficients have been computed for a polyhedral approximation of the sphere by increasing the mesh accuracy and it has been remarked that the coefficients approch zero when increasing the accuracy.
- All the derivatives have been validated by finite difference on simple models, like a cube, and on more complex polyhedra, like asteroids (433) Eros and (16) Psyche.
- Derivatives and coefficients have been validated by verifying the properties of the coefficients. In particular, when the polyhedral body is simply scaled of a factor s without scaling the normalizing radius a, the integrands $\bar{\boldsymbol{\phi}}_{n,m}$ are multiplied for s^n as they are homogeneous polynomial of degree n in the Cartesian coordinates [14]. As a consequence, also the spherical harmonics coefficients $\bar{\boldsymbol{\Phi}}_{n,m}$ verify the same property. This has been tested in a computer environment and the two computed coefficients, i.e. before and after the scaling, are consistent with the scaling procedure with machine precision. The derivatives of this procedure has been validated through finite differences.

10 Results

In this section the model is validated using the shape of asteroid (16) Psyche computed from radio observations [31], whose shape is shown in Figure 2. By applying the covariance regularization previously defined, a Monte-Carlo simulation was carried out so as to validate the model with respect to variations of σ and l. A realization of the perturbed shape is shown in Figure 3 where the nominal shape is depicted in red.

Different values of l and σ are investigated to understand the limitation of the proposed linearized model with respect to the non-linear counterpart. In Figures 4a - 4d the 1000 Monte-Carlo realizations are shown in comparison with the non-perturbed nominal shape, in red, as projected in the $x-y$ plane for different values of σ. It is clearly visible, as expected, that the shape perturbation increases as the standard deviation gets larger. A maximum 3σ of 30 km is chosen as it represents a sizable fraction of the reference radius $a = 140$ km. The input settings for the Monte-Carlo simulation are shown in Table 1 where the values of σ have been chosen to obtain a consistent logarithmic spacing in base 10.

Before presenting the validation results, a comment must be made on how the spherical harmonics coefficients are compared with the estimated uncertainties. At first glance, it seems reasonable to introduce a way to compare the global trend of the spherical harmonics coefficients uncertainty as the

number of the aforementioned coefficients increase rapidly with the degree and order of the gravity field. In the particular case of considering the same order and degree for the gravity field, the overall number of coefficients is $N^2 + 3N + 2$. This summation includes the coefficients $\bar{\boldsymbol{\Phi}}_{0,0}$ and coefficients $\bar{S}_{n,0} = 0$ for $\forall n \in [1,\, N]$.

As the spherical harmonics are the Fourier expansion on the sphere of the function representing the gravity potential [2], it is possible to characterize the gravity potential power spectrum from the coefficients. The power spectrum of the gravity on the degree n is defined as [22]:

$$\sigma_n = \sqrt{\frac{\sum_m C_{n,m}^2 + S_{n,m}^2}{2n+1}} = \sqrt{\frac{\sum_m \bar{\boldsymbol{\Phi}}_{n,m}^T \bar{\boldsymbol{\Phi}}_{n,m}}{2n+1}} = \sqrt{\frac{\bar{\boldsymbol{\Phi}}_n^T \bar{\boldsymbol{\Phi}}_n}{2n+1}} \tag{82}$$

where $\bar{\boldsymbol{\Phi}}_n$ is the vector of all coefficients of degree n.

This power spectrum is compared with the spherical harmonics uncertainty, normally obtained from the orbit determination solution from radio tracking and optical measurements [9–11]. In the present work the uncertainties are directly deduced from the shape but the procedure is similar. To compare the uncertainty in the spherical harmonics from the Monte-Carlo simulation and the linearized approach, the uncertainty of the coefficients of degree n must be defined.

For the linear approach, the uncertainty $\sigma_{n_{\text{Lin}}}$ is defined as follows:

$$\sigma_{n_{\text{Lin}}} = \sqrt{\text{Tr}\left([P_{\boldsymbol{\Phi_n}}]\right)} \tag{83}$$

where $[P_{\boldsymbol{\Phi_n}}] = \mathbb{E}\left\{\delta\bar{\boldsymbol{\Phi}}_n \delta\bar{\boldsymbol{\Phi}}_n^T\right\}$ is the block matrix that consider the covariance only of the coefficients of degree n with themselves. The size of this matrix is defined by the number of coefficients of degree n: having fixed n, the matrix size is $2\,(n+1) \times 2\,(n+1)$. This matrix can directly be extracted from $[P_{\boldsymbol{\Phi}}]$.

For the Monte-Carlo simulation, the uncertainty $\sigma_{n_{\text{MC}}}$ can be simply defined as:

$$\sigma_{n_{\text{MC}}} = \sqrt{\sum_m \sigma_{n,m}^2} \tag{84}$$

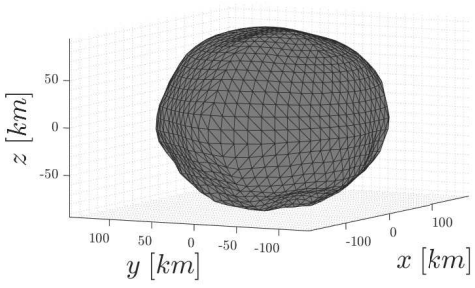

Fig. 2: The polyhedral model of asteroid (16) Psyche

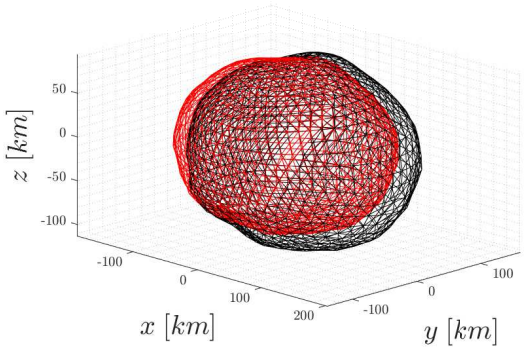

Fig. 3: The polyhedral model of asteroid (16) Psyche, in red, and one realization of the stochastic shape, in black, when $\sigma = 10$ km and $l = 100$ km

Table 1: Setting for the Monte-Carlo simulation for asteroid (16) Psyche. “Dimensions" refers to the semi-major axes of the approximating ellipsoid.

Dimensions [km]	l [km]	σ [km]	a [km]	$\rho\ \left[\frac{\text{kg}}{\text{m}^3}\right]$	MC Samples
$139.5 \times 116 \times 94.5$	{50, 75, 100}	{0.1, 0.46416, 2.5144, 10}	140	4500	1000

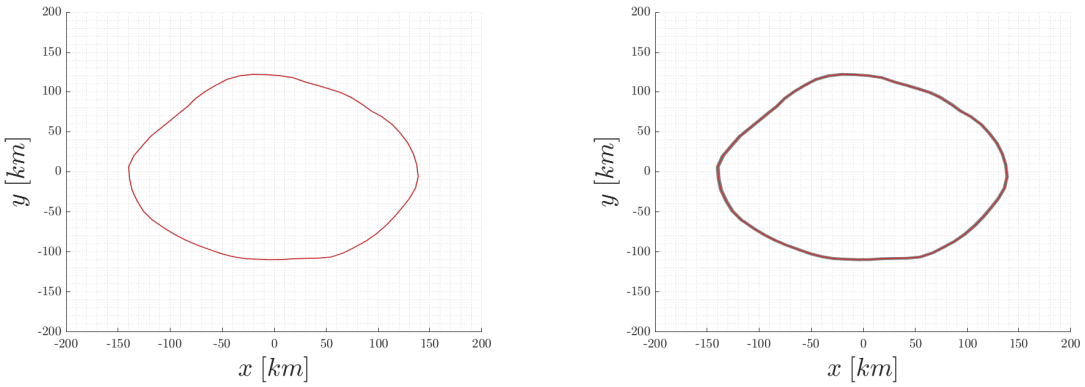

(a) $\sigma = 0.1$ km

(b) $\sigma = 0.46416$ km

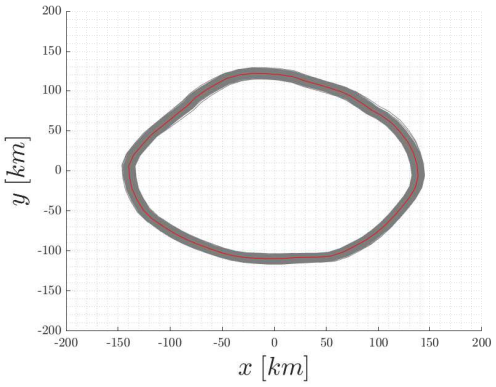

(c) $\sigma = 2.1544$ km

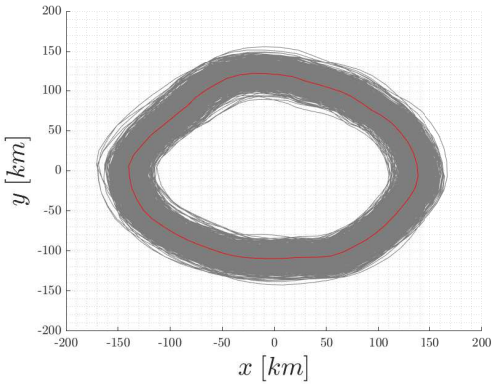

(d) $\sigma = 10$ km

Fig. 4: The intersection of the 1000 Monte-Carlo realizations with the $x - y$ plane for different values of σ when $l = 100$ km. In red, the intersection of the nominal shape with the same plane is underlined.

where $\sigma_{n,m}$ is the covariance of the coefficients of degree n and order m in a Monte-Carlo framework.

Finally, the error between the Monte-Carlo simulation and the linearized one is given by the following formula:

$$\varepsilon_{n_{\mathrm{MC/Lin}}} = \frac{|\sigma_{n_{\mathrm{MC}}} - \sigma_{n_{\mathrm{Lin}}}|}{|\sigma_{n_{\mathrm{MC}}}|} \tag{85}$$

In Figures 5a and 5b, the power spectrum σ_n is compared with the Monte-Carlo uncertainties $\sigma_{n_{\mathrm{MC}}}$ to provide the reader with a measure of the confidence it can be associated to each degree n when the shape is perturbed by varying standard deviation σ. When $\sigma_{n_{\mathrm{MC}}}$ is equal to σ_n, the uncertainty in the nth degree spherical harmonics coefficient is 100% of its magnitudes.

In Figures 6a and 6b the error is shown by fixing the perturbation length l as shown in Table 1. By looking at the figures, the error is under the 2% for small perturbation of the nominal shape while the error starts increasing when $\sigma = 10$ km. Two remarks must be made about the case $\sigma = 10$ km. First, it can be noticed from Figure 6a and 6b that the error is bigger in the higher degree coefficients as the recursive equations that define them are more and more non-linear with increasing degree. This implies that the linear approximation is breaking down for higher degree coefficients by keeping the error lower for low degree coefficients. By increasing the value of σ it is expected to have higher errors even at lower degree coefficients. Second, by looking at Figures 5a and 5b, it is clear that the shape uncertainties for the $\sigma = 10$ km have a higher value than the power spectrum of the spherical harmonics coefficients and, as a consequence, the coefficients computation provided by the nominal shape is not trustworthy

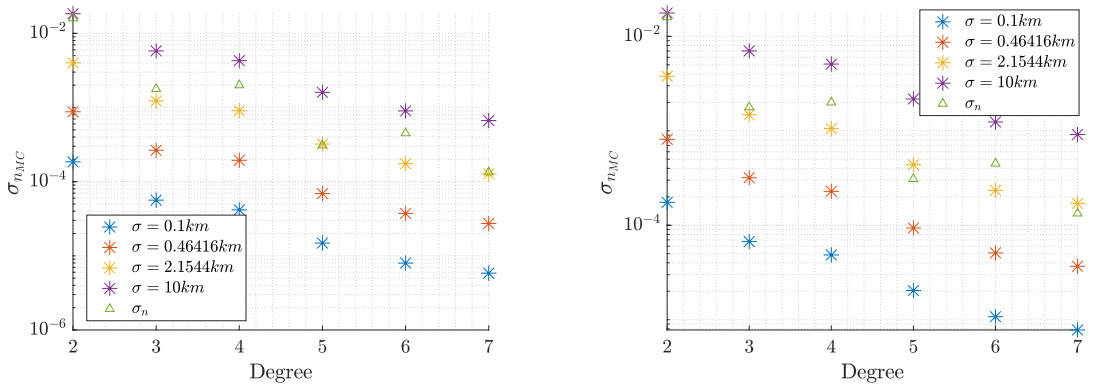

(a) $l = 100$ km (b) $l = 75$ km

Fig. 5: The Monte-Carlo uncertainty compared with the power spectrum of the spherical harmonic expansion by varying σ for different values of l. When $\sigma_{n_{\mathrm{MC}}}$ is equal to σ_n, the uncertainty in the nth degree spherical harmonics coefficient is 100% of its magnitudes. See Equations 82 and 84 for the definition of the power spectrum and Monte-Carlo uncertainty.

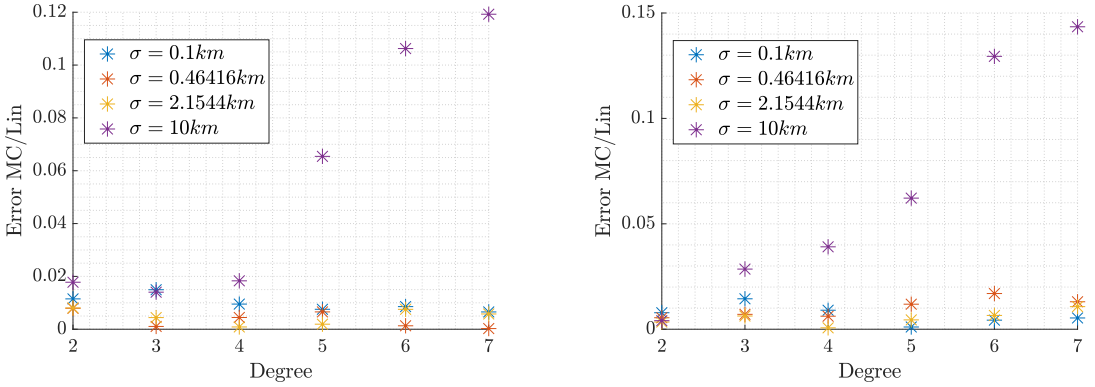

(a) $l = 100$ km (b) $l = 75$ km

Fig. 6: The error between the Monte-Carlo simulation and the linearized solution when the uncertainties are compared by varying σ for different values of l. See Equation 85 for the definition of the error.

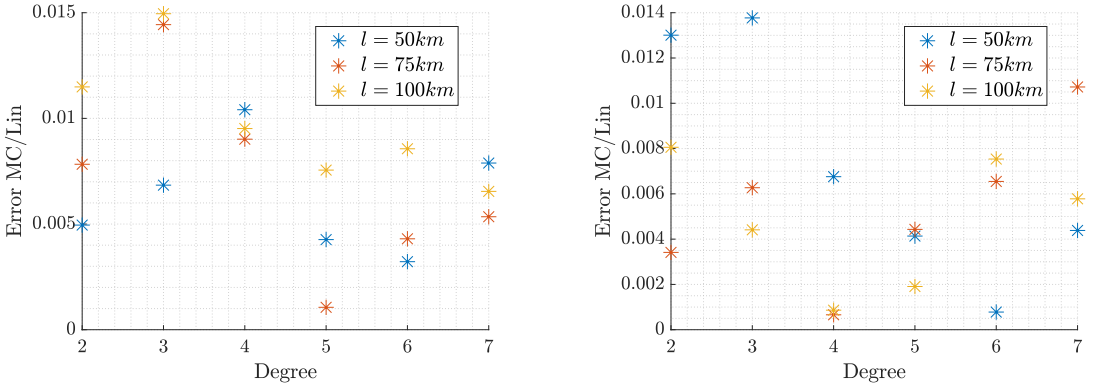

(a) $\sigma = 0.1$ km (b) $\sigma = 2.1544$ km

Fig. 7: The error between the Monte-Carlo simulation and the linearized solution when the uncertainties are compared by varying l for different values of σ. See Equation 85 for the definition of the error.

anymore. This means that the shape uncertainty makes the spherical harmonics coefficients not usable for orbit design and propagation as their power spectra have uncertainties that are 100% or higher than the value computed from the shape. Moreover, by looking at Figures 6a and 6b, it can be noticed that the linearized uncertainty model breaks down with respect to the non-linear one when the Monte-Carlo uncertainties have a higher value than the power spectra of the nominal shape spherical harmonics. As a consequence, the linearized uncertainty quantification seems a valuable tool to rapidly compute the usability of a certain degree of spherical harmonics coefficient by comparing the linearized uncertainty with the power spectrum computed from the nominal shape.

In Figures 7a and 7b the same plots are presented by fixing the value of σ. The influence of the perturbation length l seems not to drastically change the results and a pattern is not clearly shown. The perturbation length l is not directly affecting the uncertainty in the overall shape but it is influencing the interconnection among the polyhedral shape vertices by ensuring a smooth variation among adjacent vertices.

After having validated the linearized approach for uncertainty quantification in the spherical harmonics coefficients, the linearized approach is used to deduce a map of the normalized uncertainty in the gravity potential and gravity acceleration. In order to give an idea of the uncertainty in the potential and in the acceleration with respect to the nominal value, the normalized uncertainties are expressed as follows:

$$\bar{\sigma}_U(\boldsymbol{r}) = \frac{\sqrt{P_U(\boldsymbol{r})}}{U(\boldsymbol{r})} \tag{86}$$

$$\bar{\sigma}_{\boldsymbol{a}}(\boldsymbol{r}) = \frac{\sqrt{\mathrm{Tr}\left([P_{\boldsymbol{a}}](\boldsymbol{r})\right)}}{|\boldsymbol{a}(\boldsymbol{r})|} \tag{87}$$

where the potential variance and the acceleration covariance matrix are deduced from Equations 58 and 75. It must be noted that the stochastic variables are the points' position that form the polyhedral shape. As a consequence, the normalized uncertainties $\bar{\sigma}_U$ and $\bar{\sigma}_{\boldsymbol{a}}$ are functions of the point $\boldsymbol{r}$ where they are evaluated. The incorporation of the uncertainty in the position in the presented model is out of the scope of the present work but could be performed with a fashion similar to the one used for the uncertainty quantification caused by the stochastic shape.

In Figures 8a and 8b the normalized uncertainties are shown as functions of the latitude and longitude on a sphere of radius $r_{\mathrm{sph}} = a + 10$ km for the value of $\sigma = 2.1544$ km and $l = 100$ km. The value of σ has been chosen as it is the highest value where, by looking at previous validation simulations, the Monte-Carlo and the linearized approach agree. The radius r_{sph} has been chosen in order to ensure that all the possible Brillouin spheres, which dilate and contract when the shape is stochastic, are contained inside the aforementioned sphere. Figures 8a - 8b show zones, in particular in proximity of the x-axis which is located at 0° latitude and 0°/180° longitude, where the uncertainty is higher. This is caused by a coupling of the shape and the covariance $[P_{\boldsymbol{C}}]$. On the one hand, the sphere is closer to the body on the x-axis (see Table 1 for the semi-major axes of the approximating ellipsoid) and this zone of the field is more affected by the high-degree spherical harmonics, which are more ucertain in a relative sense (see Figure 5a). On the other hand, the chosen covariance is quite uniformly spread as all the points are perturbed by the same standard deviation. This implies that the highest uncertainty is localized closer to the body, thus higher uncertainties are located on the x-axis..

In Figures 9a - 9f the normalized uncertainties in the gravity potential and gravity acceleration are shown in the different Cartesian planes where the white shape is the projection of nominal shape of asteroid (16) Psyche. The normalized uncertainties are consistent with the expected results. Firstly, the normalized uncertainties are decreasing with the distance to the small body by tending to the values given by the variation in volume caused by the shape perturbation. This is due to the fact that the associated and derived Legendre polynomials decrease rapidly with the distance and the only term that remains is the Keplerian potential and acceleration. Secondly, the highest uncertainties are concentrated close to the surface where the high degree coefficients, and thus the highest uncertainties, have the most impact. At the same time, it must be noticed that, as widely known, the spherical harmonics expansion

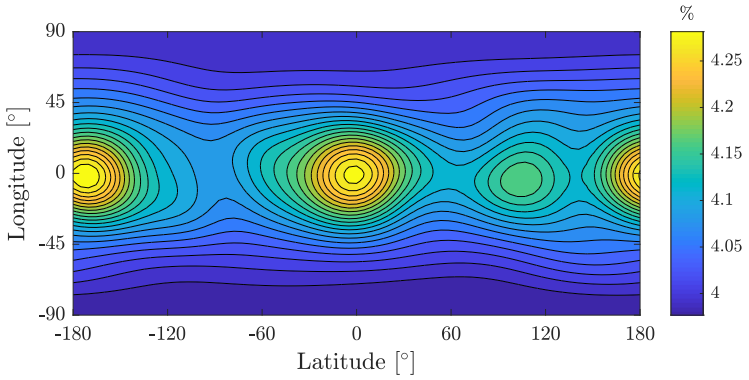

(a) Gravity potential

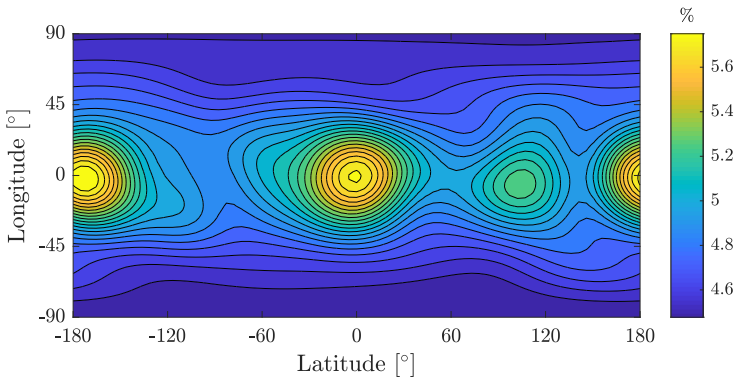

(b) Gravity acceleration

Fig. 8: The normalized uncertainties, in percentage, on the (16) Psyche gravity potential and acceleration for a 7×7 gravity field for $\sigma = 2.1544$ km as it computed on a sphere of radius $r_{\text{sph}} = a + 10$ km by varying latitude and longitude. See Equations 86 and 87 for the definition of the normalized uncertainties.

does not correctly represent the gravity field inside the Brillouin sphere [27] and results computed in this region should be interpreted carefully.

11 Conclusion

This paper presents the computation of the partial derivatives of the gravity spherical harmonics coefficients with respect to a polyhedron vertices' coordinates. First, a review of the computation of the spherical harmonics coefficients derived from a polyhedral shape is presented. The problem has been reformulated from a different point of view in order to facilitate the computation of the partial derivatives and to avoid numerical underflow problems. By starting from this new reformulation, the partial derivatives with respect to the polyhedral shape have been computed and the spherical harmonics coefficients uncertainty quantification has been presented. Moreover, the gravity potential and acceleration with a spherical harmonics representation have been reviewed and the associated uncertainty characterized. Finally results have been shown both to validate the current approach and to give examples of the possible engineering and scientific applications. The proposed method has numerous applications: maps of gravity uncertainty can be useful to mission analysts designing orbits; the shape-derived uncertainty in the spherical harmonics coefficients could be used to initialize orbit determination filters ; and the estimated spherical harmonics coefficients from the orbit determination process could be compared

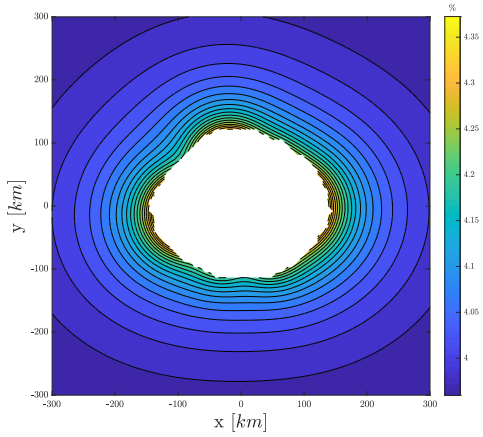

(a) Gravity potential

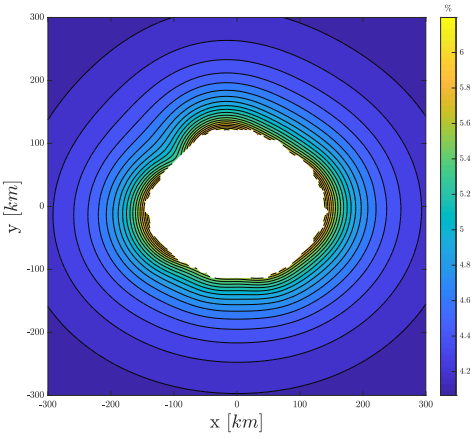

(b) Gravity acceleration

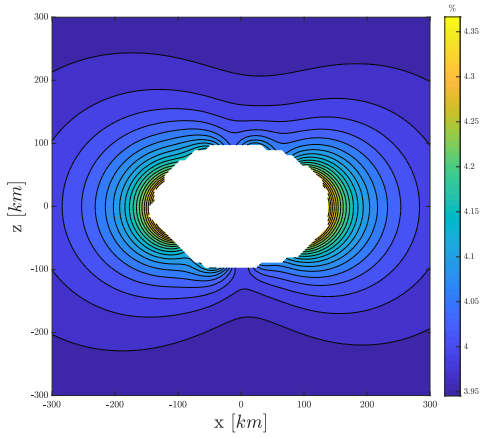

(c) Gravity potential

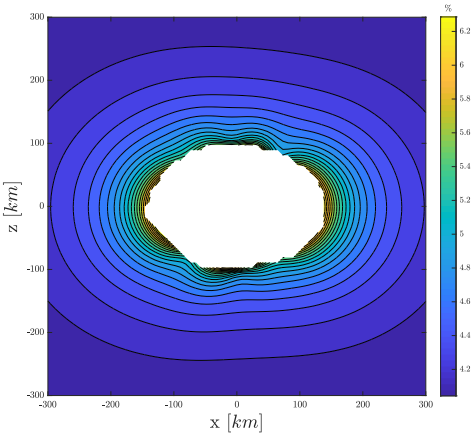

(d) Gravity acceleration

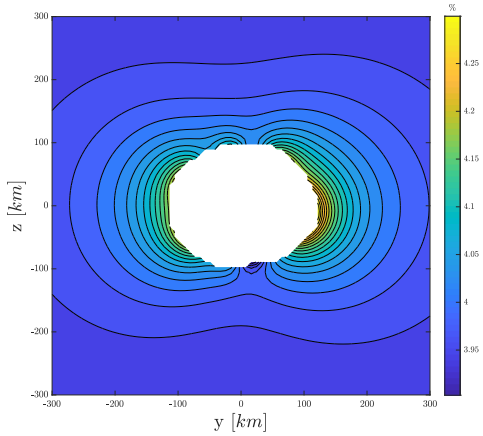

(e) Gravity potential

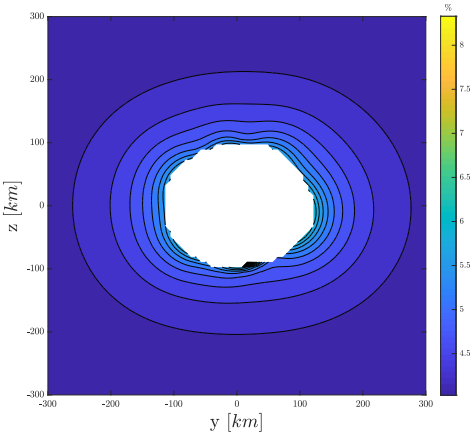

(f) Gravity acceleration

Fig. 9: The normalized uncertainties, in percentage, in the (16) Psyche gravity potential and acceleration for a 7×7 gravity field for $\sigma = 2.1544$ km in the three Cartesian planes. The asteroid (16) Psyche is shown in white. See Equations 86 and 87 for the definition of the normalized uncertainties.

against their associated shape-induced uncertainties to understand the potential source of discrepancy, which may arise from the inhomogeneity in the body's density distribution or the shape mismodeling. Moreover, the present study could give a valuable framework to understand how the dynamical state of an object evolves when subjected to an uncertain shape, thus an uncertainty gravity field.

12 Acknowledgment

Paolo Panicucci would like to express his gratitude to CNES, the Fondation ISAE-SUPAERO, the ISAE SUPAERO and Airbus Defence & Space for funding this research under the contract CNES-2879. Benjamin Bercovici and Jay McMahon would like to express their thanks to NASA for funding this work under the grant PDART NNX16AG50G. The authors thank the reviewers for the comments that helped to improve the clarity of the work.

Conflict of interest

The authors declare not to have any conflict of interest.

References

1. Claus Müller. *Spherical harmonics*, volume 17. Springer, 2006.
2. Volker Michel. *Lectures on constructive approximation: Fourier, spline, and wavelet methods on the real line, the sphere, and the ball*. Springer Science & Business Media, 2012.
3. Willi Freeden and Ulrich Windheuser. Combined spherical harmonic and wavelet expansion — A future concept in Earth's gravitational determination. *Applied and Computational Harmonic Analysis*, 4(1):1–37, 1997.
4. Yu Takahashi, Daniel Jay Scheeres, and Robert A Werner. Surface gravity fields for asteroids and comets. *Journal of guidance, control, and dynamics*, 36(2):362–374, 2013.
5. William Duncan MacMillan. The theory of the potential. 1958.
6. Robert A Werner and Daniel J Scheeres. Exterior gravitation of a polyhedron derived and compared with harmonic and mascon gravitation representations of asteroid 4769 Castalia. *Celestial Mechanics and Dynamical Astronomy*, 65(3):313–344, 1996.
7. Xuanyu Hu and Christopher Jekeli. A numerical comparison of spherical, spheroidal and ellipsoidal harmonic gravitational field models for small non-spherical bodies: examples for the Martian moons. *Journal of Geodesy*, 89(2):159–177, 2015.
8. Yu Takahashi and DJ Scheeres. Small body surface gravity fields via spherical harmonic expansions. *Celestial Mechanics and Dynamical Astronomy*, 119(2):169–206, 2014.
9. AS Konopliv, SW Asmar, RS Park, BG Bills, F Centinello, AB Chamberlin, A Ermakov, RW Gaskell, N Rambaux, CA Raymond, et al. The Vesta gravity field, spin pole and rotation period, landmark positions, and ephemeris from the dawn tracking and optical data. *Icarus*, 240: 103–117, 2014.
10. AS Konopliv, RS Park, AT Vaughan, BG Bills, SW Asmar, AI Ermakov, N Rambaux, CA Raymond, JC Castillo-Rogez, CT Russell, et al. The Ceres gravity field, spin pole, rotation period and orbit from the Dawn radiometric tracking and optical data. *Icarus*, 299:411–429, 2018.
11. James K Miller, AS Konopliv, PG Antreasian, JJ Bordi, S Chesley, CE Helfrich, WM Owen, TC Wang, BG Williams, DK Yeomans, et al. Determination of shape, gravity, and rotational state of asteroid 433 Eros. *Icarus*, 155(1):3–17, 2002.
12. Bernard Godard, Frank Budnik, Pablo Muñoz, Trevor Morley, and Vishnu Janarthanan. Orbit determination of Rosetta around comet 67P Churyumov-Gerasimenko. In *Proceedings 25th International Symposium on Space Flight Dynamics–25th ISSFD, Munich, Germany*, 2015.
13. Nicola Baresi and Daniel J Scheeres. Bounded relative motion under zonal harmonics perturbations. *Celestial Mechanics and Dynamical Astronomy*, 127(4):527–548, 2017.

14. Robert A Werner. Spherical harmonic coefficients for the potential of a constant-density polyhedron. *Computers & Geosciences*, 23(10):1071–1077, 1997.
15. JCP Melman, E Mooij, and R Noomen. State propagation in an uncertain asteroid gravity field. *Acta Astronautica*, 91:8–19, 2013.
16. Yu Takahashi and Daniel Jay Scheeres. Small-body postrendezvous characterization via slow hyperbolic flybys. *Journal of guidance, control, and dynamics*, 34(6):1815–1827, 2011.
17. Benjamin Bercovici, Paolo Panicucci, and Jay W McMahon. Analytical shape uncertainties in the polyhedron gravity model. *Celestial Mechanics and Dynamical Astronomy*, Under Review.
18. Benjamin Bercovici and Jay W McMahon. Inertia parameter statistics of an uncertain small body shape. *Icarus*, 328:32–44, 2019.
19. K Muinonen. Introducing the Gaussian shape hypothesis for asteroids and comets. *Astronomy and Astrophysics*, 332:1087–1098, 1998.
20. Hanspeter Schaub and John L Junkins. *Analytical mechanics of space systems*. American Institute of Aeronautics and Astronautics, 2005.
21. Ian Moffat Smith, Denwood Vaughan Griffiths, and Lee Margetts. *Programming the finite element method*. John Wiley & Sons, 2013.
22. William M Kaula. *Theory of satellite geodesy: applications of satellites to geodesy*. Courier Corporation, 2013.
23. Leland E Cunningham. On the computation of the spherical harmonic terms needed during the numerical integration of the orbital motion of an artificial satellite. *Celestial Mechanics*, 2(2): 207–216, 1970.
24. Robert G Gottlieb. Fast gravity, gravity partials, normalized gravity, gravity gradient torque and magnetic field: derivation, code and data. 1993.
25. Simon A Holmes and Will E Featherstone. A unified approach to the Clenshaw summation and the recursive computation of very high degree and order normalised associated legendre functions. *Journal of Geodesy*, 76(5):279–299, 2002.
26. Brandon Allan Jones. Efficient models for the evaluation and estimation of the gravity field. 2010.
27. Daniel J Scheeres. *Orbital motion in strongly perturbed environments: applications to asteroid, comet and planetary satellite orbiters*. Springer, 2016.
28. Karri Muinonen and Tuomo Pieniluoma. Light scattering by gaussian random ellipsoid particles: first results with discrete-dipole approximation. *Journal of Quantitative Spectroscopy and Radiative Transfer*, 112(11):1747–1752, 2011.
29. Martin Berz. Modern map methods in particle beam physics. 1999.
30. RW Gaskell. Gaskell eros shape model v1. 0. *NASA Planetary Data System*, 96, 2008.
31. Michael K Shepard, James Richardson, Patrick A Taylor, Linda A Rodriguez-Ford, Al Conrad, Imke de Pater, Mate Adamkovics, Katherine de Kleer, Jared R Males, Katie M Morzinski, et al. Radar observations and shape model of asteroid 16 Psyche. *Icarus*, 281:388–403, 2017.
32. Samuel Pines. Uniform representation of the gravitational potential and its derivatives. *AIAA Journal*, 11(11):1508–1511, 1973.
33. Richard H Rapp. A Fortran program for the computation of gravimetric quantities from high degree spherical harmonic expansions. Technical report, Ohio State University Columbus Department of Geodetic Science and Surveying, 1982.
34. John B Lundberg and Bob E Schutz. Recursion formulas of Legendre functions for use with nonsingular geopotential models. *Journal of Guidance, Control, and Dynamics*, 11(1):31–38, 1988.

A Associated and Derived Legendre function

The gravity potential and acceleration require the computation of associated Legendre functions (ALF) and derived Legendre functions (DLF). The use of ALF in gravity potential is gathered directly from the solution of the Laplace equation [5] while the use of the DLF is a reformulation of the potential given by Pines [32] and then reused by Gottlieb [24].

The definition of the ALF and DLP is the following [24, 25]:

$$\bar{P}_{n,m}(x) = N_{n,m}(1-x^2)^{\frac{m}{2}} \frac{\mathrm{d}^m}{\mathrm{d}x^m} P_n(x) \tag{88}$$

$$\bar{P}_n^m(x) = N_{n,m} \frac{\mathrm{d}^m}{\mathrm{d}x^m} P_n(x) \tag{89}$$

where:

$$P_n(x) = \frac{1}{2^n\, n!} \frac{\mathrm{d}^n}{\mathrm{d}x^n}(x^2-1)^n \tag{90}$$

is the Legendre polynomial of degree n. The factor $N_{n,m}$ is the normalization factor introduced by Kaula [22] that is given by the following formula:

$$N_{n,m} = \sqrt{\frac{(n-m)!\,(2n+1)\,(2-\delta_{0\,m})}{(n+m)!}} \tag{91}$$

Several recursive formulas exist for the derivation of ALP and DLP [25, 33]. In this section the formulas used in the present work are reported.

The ALP are computed with the following recursive algorithm [33]:

$$\begin{aligned}
\bar{P}_{0,0}(x) &= 1 \\
\bar{P}_{1,0}(x) &= \sqrt{3}\,x \\
\bar{P}_{1,1}(x) &= \sqrt{3} \\
\bar{P}_{n,n}(x) &= \sqrt{\frac{2n+1}{2n}}\,\bar{P}_{n-1,n-1} \\
\bar{P}_{n,n-1}(x) &= \sqrt{2n+1}\;x\;\bar{P}_{n-1,n-1} \\
\bar{P}_{n,m}(x) &= \urcorner_{n,m}\, x \bar{P}_{n-1,m} - \frac{\urcorner_{n,m}}{\urcorner_{n-1,m}} \bar{P}_{n-2,m}
\end{aligned} \tag{92}$$

where the last formula is valid if $m < n-1$. Furthermore:

$$\urcorner_{n,m} = \sqrt{\frac{(2n+1)\,(2n-1)}{(n-m)\,(n+m)}} \tag{93}$$

The DLP are recursively computed in the same fashion [34]:

$$\begin{aligned}
\bar{P}_0^0(x) &= 1 \\
\bar{P}_1^0(x) &= \sqrt{3}\,x \\
\bar{P}_1^1(x) &= \sqrt{3}\sqrt{1-x^2} \\
\bar{P}_n^n(x) &= \sqrt{\frac{2n+1}{2n}}\,\bar{P}_{n-1}^{n-1} \\
\bar{P}_n^{n-1}(x) &= \sqrt{2n+1}\;x\;\bar{P}_{n-1}^{n-1} \\
\bar{P}_n^m(x) &= \urcorner_{n,m}\, x \bar{P}_{n-1}^m - \frac{\urcorner_{n,m}}{\urcorner_{n-1,m}} \bar{P}_{n-2}^m
\end{aligned} \tag{94}$$

where the last formula is valid if $m < n-1$.